EUROPEAN FUSION DEVELOPMENT AGREEMENT

EFDA–JET–PR(01)104

S. Jachmich, G. Maddison, M.N.A. Beurskens, P. Dumortier, T. Eich,A. Messiaen, M.F.F. Nave, J. Ongena, J. Rapp, J. Strachan, M. Stamp, G. Telesca, B. Unterbergand contributors to the EFDA-JET workprogramme

Seeding of Impurities in JET H-Mode Discharges to Mitigate the Impact of ELMs

Seeding of Impurities in JET H-Mode Discharges to Mitigate the Impact of ELMs

S. Jachmich[1], G. Maddison[2], M.N.A. Beurskens[3], P. Dumortier[1], T. Eich[4], A. Messiaen[1], M.F.F. Nave[5], J. Ongena[1], J. Rapp[6], J. Strachan[7], M. Stamp[2], G. Telesca[8], B. Unterberg[6]
and contributors to the EFDA-JET workprogramme*

[1]Laboratory for Plasmaphysics, Ecole Royale Militaire/Koninklijke Militaire School, EURATOM-Association "Belgian State", Brussels, Belgium[+]
[2]EURATOM/UKAEA Fusion Association, Culham, UK
[3]FOM-Instituut voor plasmafysica 'Rijnhuizen', Euratom-Association, Nieuwegein, The Netherlands[+]
[4]Max-Planck Institut fuer Plasmaphysik, Euratom Association, Garching, Germany
[5]CFN, Euratom-IST Ass., Lisbon, Portugal
[6]Institut f¸r Plasmaphysik, Euratom-Association, Forschungszentrum Jülich, Jülich, Germany[+]
[7]Princeton Plasma Physics Laboratory, Princeton, USA
[8]Associazione Euratom, Consorzio RFX, Padua, Italy
[+]Partners in the Trilateral Euregio Cluster (TEC)
** See annex of J. Pamela et al, "Overview of Recent JET Results and Future Perspectives", Fusion Energy 2000 (Proc. 18th Int. Conf. Sorrento, 2000), IAEA, Vienna (2001).*

Paper to be submitted for publication in PPCF

ABSTRACT

ELMy H-mode is one of the foreseen operational scenarios for ITER-FEAT. Good confinement and density is usually associated with Type I ELMs, which, however, will have a severe impact on the divertor target plates in ITER. At the JET-tokamak impurities have been seeded into a variety of discharge configurations, by which the radiation level can be risen by a factor of 2. This delays the appearance of ELMs and reduces the power load onto the divertor target plates. In this paper the influence of the impurities on the ELM behaviour and the plasma edge properties will be discussed. Several divertor diagnostics, such as electrical probes and infra-red camera indicate a reduction of the heat power load at the inner divertor target tiles and a shrinking of the impact zone at the outer divertor.

1. INTRODUCTION

The seeding of inert gases has been demonstrated to be beneficial for the formation of a radiating belt to lower the heat fluxes to the plasma facing components and concomitantly good confinement properties have been observed in several machines [1,2]. Four different discharge types with impurity seeding have been performed at the JET-tokamak: (i) at low triangularity (δ•H 0.2) (SLT), (ii) at high triangularity (δ•H 0.3) (SHT), both with the X-point located on the septum, and (iii) with the divertor strike points on the vertical targets (VT) and (iv) at extremely high triangularity (δ•H 0.4) in a configuration close to the one projected for ITER, (EHT). The locations of the strike points in the different divertor configurations and the measuring positions of the diagnostics used in this paper are shown in Figure 1.

In the septum (SLT, SHT) and the vertical target discharges (VT) three different confinement phases can be distinguished. A first phase, where sufficient auxiliary heating is applied to enter the H-mode regime (Fig. 2); a second phase where the density is built up by a strong gas puff of D_2 causing a confinement reduction ("puff" phase) with additional impurity seeding (of e.g. argon), in order to raise the radiation level; and finally a third phase when the D_2 gas valve is closed ("afterpuff" phase) during which confinement recovers to high values. To maintain the density in this phase, small levels of D_2 puff are applied in addition to a modest extra amount of argon. This leads to quasi-stationary plasmas at high densities close to the Greenwald level and simultaneously good confinement ($H_{98(y,2)}$•H 0.95). These three phases will be discussed for a seeded SLT and its unseeded reference discharge in section 2.1.

In the discharges at extremely high triangularity (EHT), there is no distinction between a "puff" and "afterpuff" phase, as the confinement in these discharges is rather robust against strong gas puffing, and therefore a continuous D puff is applied. More details on the confinement properties of impurity seeded discharges can be found in [3-5].

A new confinement scenario is only attractive as a possible operational scheme, if the effects caused by ELMs on the first wall are acceptable. Therefore first the link between the global confinement and ELMs will be discussed, and then results on changes in the SOL power flux will be given. This paper will mainly deal with the effects of impurities on ELMs in the afterpuff of low

δ septum discharges, and where necessary compare with high triangularity discharges and vertical target discharges at low triangularity.

2. GLOBAL ELM BEHAVIOUR AND CHANGES IN EDGE PROFILES IN IMPURITY SEEDED ELMY H-MODE DISCHARGES

2.1 LOW TRIANGULARITY

2.1.1 Puff phase

Figure 2 compares a seeded and an unseeded septum discharge at low triangularity; numerical values for different parameters of these discharges are summarised in Table 1. Strong gas puffing leads to a confinement degradation, which is associated with an increase in the frequency of the Type I ELMs and, depending on the intensity of the deuterium gas puff, the appearance of Type III ELMs. When argon is puffed in addition to deuterium in this puff phase, the confinement degradation is even stronger and the ELM-frequency increases further. This can be understood as the result of the enhanced radiation (about 50% higher for seeded pulses) and hence a lowered edge electron temperature (Fig. 3), which reduces the pedestal energy. Note that the diamagnetic plasma energy is also smaller in the puff phase compared to the unseeded pulse, since the density remains about the same. Once the D gas-puff is stopped, the ELM frequency decreases and Type I ELMs appear. This observation is consistent with rising pedestal energy [4], which can be also inferred from Figure 3.

2.1.2 Afterpuff phase

During this phase of the discharge again a modest amount of argon has been seeded. This can lead, depending on the radiation level, to ELM-free phases ending with giant ELMs, or Type I ELMs with compound or regular signatures. In Figure 2 two exemplary time traces of the edge recycling inferred from a horizontal D_α measurement are displayed. The time for the next ELM to appear is larger in the seeded pulse than in the unseeded. Concomitantly the amplitude does not increase with decreasing ELM-frequency. This is caused by the enhanced radiation, which acts in two ways: first the power through the separatrix is lowered; second, the edge electron temperature is lower and so is the edge pressure gradient as illustrated in Figure 4 showing the smaller ∇p_e for seeded plasmas. The Abel-inverted radiation power profiles for the pulses illustrated in Fig. 2 show that a large fraction has been radiated in the edge (see Fig. 5), with more central radiation in the seeded discharge in the afterpuff, as the Ar seeding was not optimised for that pulse and the impurities accumulated [5]. Values of the radiated power integrated over $0.8 < r/a < 1.0$, normalised to the total radiated power, are shown in Table 1. Altogether this causes a drop in the edge electron temperature, Fig.4, and a peaking of the current profile, not shown. As a result, the stability regime for the edge profile, in the picture of a coupled peeling-ballooning mode as a trigger for the Type I ELMs [6], is enhanced and hence the ELM cycle prolonged. This is also confirmed by the observation in [7] that the appearance of the first giant ELM is delayed when an impurity is added into the discharge.

2.2. EFFECT OF SEEDING ON ELM APPEARANCE IN ALL CONFIGURATIONS

In [7] an empirical scaling of the ELM frequency has been proposed, which is also confirmed for giant ELMs using a simple model [9], where the temporal sequence of the ELMs is imposed by the reheating time. As shown in Fig. 6 the ELM frequency of seeded plasmas (closed symbols) with reduced power crossing the separatrix due to the enhanced radiation, is lower than that of their unseeded counterparts (open symbols). This behaviour has been found for all pulses analysed, independent of the details of the plasma configuration, besides the Septum-high triangularity pulses, where the effect is less pronounced.

Summarising, in the afterpuff of impurity seeded low triangularity ELMy H-Mode discharges, a reduction in edge electron temperature is found leading to a lower pedestal pressure (despite the increase in the edge density) and a lower ELM frequency. This result is also obtained in the high triangularity discharges with impurity seeding. Reduced pedestal energy W_{ped}, which is calculated from the electron pressure at the pedestal top, mitigates the energy loss per ELM ΔW_{ELM}. In [10] it has been demonstrated that the fractional energy loss ($\Delta W_{ELM}/W_{ped}$) depends on the parallel ion particle transport time $\tau_{\parallel}$ and the characteristic time of enhanced cross-field transport τ_{ELM} during an ELM:

$$\frac{\Delta W_{ELM}}{W_{ped}} = \frac{1}{1+ \tau_{\parallel}/\tau_{ELM}} \left(\frac{\Delta W_{ELM}}{W_{ped}} \right)_0 \qquad (1)$$

with $(\Delta W_{ELM}/W_{ped})_0$ as the energy loss if the transport would be infinite in the SOL. Increasing density or decreasing temperature will lead to a larger parallel transport time and hence to a smaller fractional energy loss during an ELM. Table 1 shows for the puff and afterpuff phases the respective values for an unseeded and seeded discharge. With a typical value in JET of $\tau_{ELM} \approx 0.2$ ms [10], a drop in $\Delta W_{ELM}/W_{ped}$ by 14% in the puff-phase and 24% in the afterpuff-phase can be expected. This drop is brought about by the somewhat higher edge density in combination with a reduced edge temperature resulting in a change of the collisionality and hence parallel transport time.
Using the fast magnetic diagnostic the fractional energy loss has been estimated by taking ΔW_{ELM} equal to the drop in the diamagnetic energy (ΔW_{dia}). It is seen that in many cases $\Delta W_{dia}/W_{dia}$ is smaller in the seeded discharges (Fig. 7). Shown is the relative decrease of $\Delta W_{dia}/W_{dia}$ and P_{sep} of the seeded pulse with respect to the unseeded pulse, i.e. a drop in P_{sep} by 27% has caused a drop in $\Delta W_{dia}/W_{dia}$ by 36%. In the afterpuff-phase of the cases shown one was able to lower the ELM-energy loss by raising the radiation level. However in the case of high triangularity discharges, (δ=0.4) the energy loss per ELM was not significantly lowered by the seeding. Although $(\Delta W_{ELM}/W_{ped})_0$ is not known, the seeded and unseeded pulses can be compared by considering the effect of the impurity seeding on $\Delta W_{ELM}/W_{ped}$ solely due to a change in $\tau_{\parallel}$. Note however that the contribution of the pedestal energy to the total stored diamagnetic energy is reduced in the seeded discharges. Therefore the decrease in the fractional energy loss per ELM is even larger. For the pair of discharges discussed above the expected change in $\Delta W_{dia}/W_{dia}$ would then be 32%, which is remarkably close

to the experimental value of about 35%. Both lower ELM frequency and energy loss per ELM $\Delta W_{ELM}/W_{dia}$ help to maintain or even to increase the stored energy despite the high radiation. Of course this does not answer whether some of the released energy during the ELM can be radiated away before reaching the divertor target plates.

3. EFFECTS ON THE DIVERTOR LOAD AND PARTICLE EFFLUX

3.1. AFTERPUFF PHASE OF VERTICAL TARGET PULSES

The contribution of the ELMs to the total particle losses has been determined by subtracting the steady state particle losses, defined as the particle losses in between ELMs, from the total D_α signal. The average particle loss per ELM is then found by integrating this signal over time and dividing it by the number of ELMs within the considered time interval. This quantity increases only slightly with higher radiation levels. However one should note that due to the continuous seeding, steady-state conditions have not been fully achieved and therefore even after the ELM burst additional particle losses still show up.

To determine the deposited power, in addition the surface-facing electron temperature has been measured using the divertor target triple probes. The heat flux is calculated assuming a constant sheath transmission factor of 7.8 [12]. Due to the specific location of the probes only discharges with the strike points on the vertical target plates could be analysed. Fig. 8 shows the time-integrated heat fluxes during the puff- and afterpuff-phase. The quantity r-a is the location of the probe, when mapped to the midplane. Positive values of r-a specify the SOL, negative values belong to the private flux region. It is clear that the peak of the heat flux during an ELM at the strike point is not or only slightly changed. However the reduction with respect to the unseeded reference of the ELM-peaks measured by neighbouring probes indicate a shrinking of the impact zone of the ELM burst, during the puff-phase at the outer divertor whereas the heat load at the inner strike point is significantly reduced and the wetted area is widened. In the afterpuff-phase the effects are not as pronounced as in the puff-phase, but still the heat flux to the inner divertor is lowered over the whole impact zone, whereas at the outer divertor only the width of the wetted area is reduced. Although the ion temperature is not accessible to the probes, the reduction in the power load on the outer target (not corrected for the magnetic field inclination angle) shown in Fig. 7 is corroborated by charge exchange spectroscopy measurements that indicate lower ion temperatures as well. In addition thermo-couple data confirm that the inner divertor tiles have absorbed 13% and the outer divertor tiles 16% less energy.

3.2 PUFF PHASE OF EXTREMELY HIGH TRIANGULARITY – PROBE AND IR-DATA

The benefit of the radiation to reduce the heat load in the divertor has also been seen in seeded discharges at extremely high triangularity (Fig. 9). The seeding has been applied from t=60.5 sec on. After the radiation level has increased, the slope of the incremental heat flux flattens. At this stage of the discharge, the outer divertor is about to pass the attachment limit (figure 10), where the

degree of detachment (DoD) inferred from the ion saturation current of a Langmuir probe, which resides at the strike point. The DoD is the ratio between the expected ion saturation current J_{sat}^{scal}, when the plasma would stay attached, and the measured ion saturation current J_{sat}^{meas}:

$$DoD = \frac{J_{sat}^{scal}}{J_{sat}^{meas}} \qquad \text{with } J_{sat}^{scal} = \gamma \langle \bar{n}_e \rangle^2$$

Since the ion saturation current should increase with the density, its scaling is determined during the density rise at the beginning of the puff phase. By this the constant γ has been determined experimentally to be $2x10^{-35}$. When the DoD becomes larger than 2, partial detachment has been achieved [13]. Later at t=62.0 sec the radiated power increases again, the outer divertor now clearly detaches partially and the heat flux caused by the ELMs diminishes further. Whether total detachment is present, cannot be determined due to the lack of spatial information on the ion fluxes to the outer divertor. At t=62.7 sec the radiation limit has been reached, which causes a stop of the discharge.
Interestingly in extreme high triangularity discharges strongly reduced temperatures in the outer and inner divertor are observed with infrared measurements (Fig. 11). The power load on the inner divertor tiles could be inferred for the same discharge as in figure 10 from the surface temperature using the THEODOR code [14]. The data in figures 12 correspond to the location as indicated in Fig. 1. The reduction of the heat flux in between ELMs can be seen in Fig. 12a. The ELM peaks, which show some scatter, are on the average reduced during the seeding phase. Therefore the heat flux has been integrated in time as described in the previous section. We find that for the seeded discharge the maximum heat load during an ELM is in average reduced from 8.5 10^2 MW/m^2 to 7.2 10^2 MW/m^2. Together with the lower ELM frequency a total of 1 MJ/m^2 has been radiated away during the considered time interval of 2.1 sec (Fig. 12b). In figure 12b the time integrated heat flux to the inner strike point after subtracting the in between ELMs level, i.e. only the heat load caused by the ELM-events, is displayed. The comparison with the unseeded reference shows that heat load at the strike point can be reduced. However the width of the deposition zone, defined as the ratio of the total heat flux to the peak heat flux, tends to increase.

4. SUMMARY

Impurity seeding in tokamak plasmas aims at creating a radiating belt in order to reduce the divertor heat load. The radiation level can be raised in both the puff phase as well as in the afterpuff phase. In the puff phase Type III ELMs are present, of which frequency increases as a result of the higher radiated power. In this phase the confinement is degraded not only by the strong D_2 puffing, but also by the seeding of argon. The extremely high triangularity pulses are an exception, since the good confinement properties with Type I ELMs remain in spite of the large gas puff. The stop of the D_2 puff is followed by a recovery of the confinement and the appearance of Type I ELMs. It has been demonstrated that the behaviour of Type I ELMs in the afterpuff phase in low triangularity discharges, but also in the extremely high triangularity discharges, is affected in various ways: on one hand, the power crossing the separatrix power is smaller and a lower ELM frequency is achieved;

on the other hand, the edge pedestal for argon seeded afterpuff phases is reduced and the heat flux is diminished.

The good confinement properties seen in these discharges are augmented by the acceptable energy loss, which is lowered by up to one third, and the lower frequency of ELMs. The divertor probes have indicated in discharges, where the strike point is at the vertical target, that on the inner divertor the heat flux decreases over the whole wetted area. At the outer divertor the heat load at the strike zone remains about the same concomitantly with a shrinking of the impact zone. In the extremely high pulses the probes have shown a decreasing heat flux if the radiated power fraction decreases. This has been also confirmed by infrared camera data of the inner divertor strike zone. The absorbed energy measured by thermocouples elements, which are embedded in the divertor tiles, is lower when an impurity has been added in the discharge. Presently experimental work is underway to achieve a steady-state phase with benign ELMs by tuning the deuterium and argon gas levels.

REFERENCES

[1]. Ongena J. *et al* 1999 *Plasma Phys. Control. Fusion* **41** A379

[2]. Kubo H. *et al* 2001 *Nucl. Fusion* **41** 227

[3]. Dumortier P *et al* 2001 *Controlled Fusion and Plasma Physics* (Proc. 28th EPS Conf., Funchal 2001), submitted to *Plasma Phys. Control. Fusion*

[4]. Maddison G. *et al* 2000 *Fusion Energy* (Proc. 18th IAEA Conf. on Plasma Physics and Controlled Nuclear Fusion Research, Sorrento 2000) (Vienna: IAEA) paper IAEA-CN-77/ EX5/4

[5]. Nave F. *et al* 2001 *Controlled Fusion and Plasma Physics* (Proc. 28th EPS Conf, Funchal 2001)

[6]. Wilson H R. *et al* 1996 *Phys. Plasmas* **3** 248

[7]. Nave F. *et al* 1999 *Controlled Fusion and Plasma Physics* (Proc. 26th EPS Conf., Maastricht 1999)

[7]. Kerner W. *et al* 1997 *Plasma Phys. Control. Fusion* **39** 757

[9]. Itoh S I. *et al* 1996 *Plasma Phys. Control. Fusion* **38** 527

[10]. Janeschitz G. *et al* 2001 *J. Nucl. Mater.* **290-293** 1

[11]. Loarte A. *et al* 2001 *Controlled Fusion and Plasma Physics* (Proc. 28th EPS Conf., Funchal 2001)

[12]. Stangeby P. and Mc Cracken G 1990 *Nuclear Fusion* **32** 1225

[13]. Loarte A *et al* 1998 *Nuclear Fusion* **38** 331

[14]. Eich T *et al* 2001 *Controlled Fusion and Plasma Physics* (Proc. 28th EPS Conf., Funchal 2001)

Table 1: Comparison of ELM-relevant parameter of an unseeded and a seeded discharge. The values have been taken from to the corresponding profiles shown in Figure 3 and 4.

Pulse	seeding	$P_{rad,edge}$	n_{ped} / 10^{19} m^{-3}	T_{ped} / eV	p_{ped} / kPa	ν^*_{ped}	τ_7 / ms
53024 (puff)	unseeded	35%	~4.2 ± 0.2	~800 ± 70	5.4 ± 0.5	0.28 ± 0.05	0.40 ± 0.02
53015 (puff)	Ar	50%	~4.2 ± 0.3	~650 ± 60	4.4 ± 0.5	0.42 ±0.09	±0.51 ± 0.04
53024 (aft.p.)	unseeded	40%	~3.3 ± 0.2	~1100 ± 130	5.8 ± 0.7	0.12 ± 0.02	0.29 ±0.03
53015 (aft.p.)	Ar	40%	~3.8 ± 0.2	~ 850 ± 90	5.2 ± 0.6	0.22 ± 0.05	0.35 ± 0.03

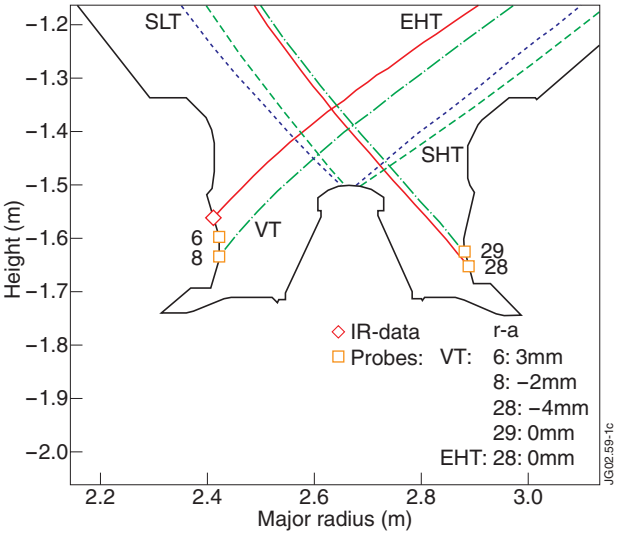

Figure 1: Separatrix location for various divertor configurations. The diamond is representing the location at which the heat fluxes, shown in Fig. 12, have been measured by an Infrared-camera. The squares correspond to the location of the divertor probes. The value r-a gives the distance of the probe to the separatrix mapped to the midplane radius.

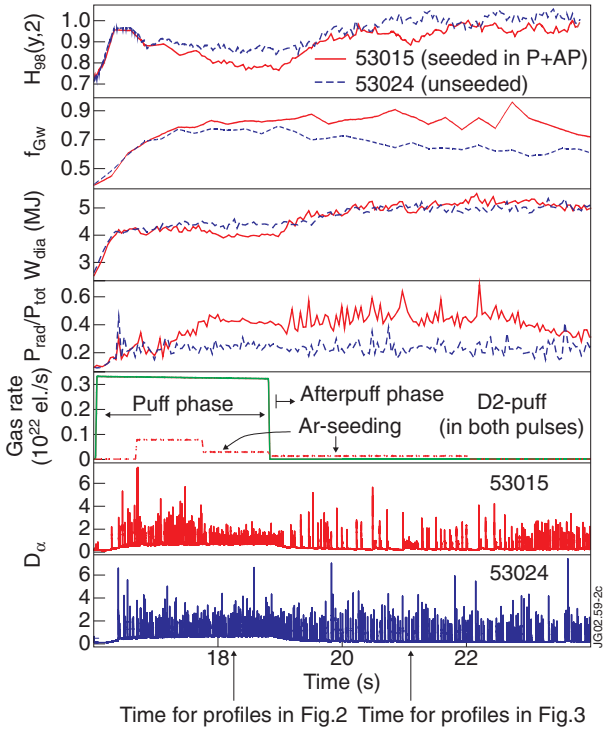

Figure 2: Comparison of unseeded discharge with argon seeded discharge in a Septum configuration with a low triangularity of 0.22. The pulses are auxiliary heated with 12 MW of NBI and 2 MW of ICRH. The seeding has been applied during the "puff" phase as well as during "afterpuff" phase. Shown are a) H98(y,2)-factor, b) Greenwald fraction, c) diamagnetic plasma energy, d) radiated power fraction, e) gas rate of deuterium and argon puff, f) D_α-trace of seeded pulse, g) D_α-trace of unseeded pulse.

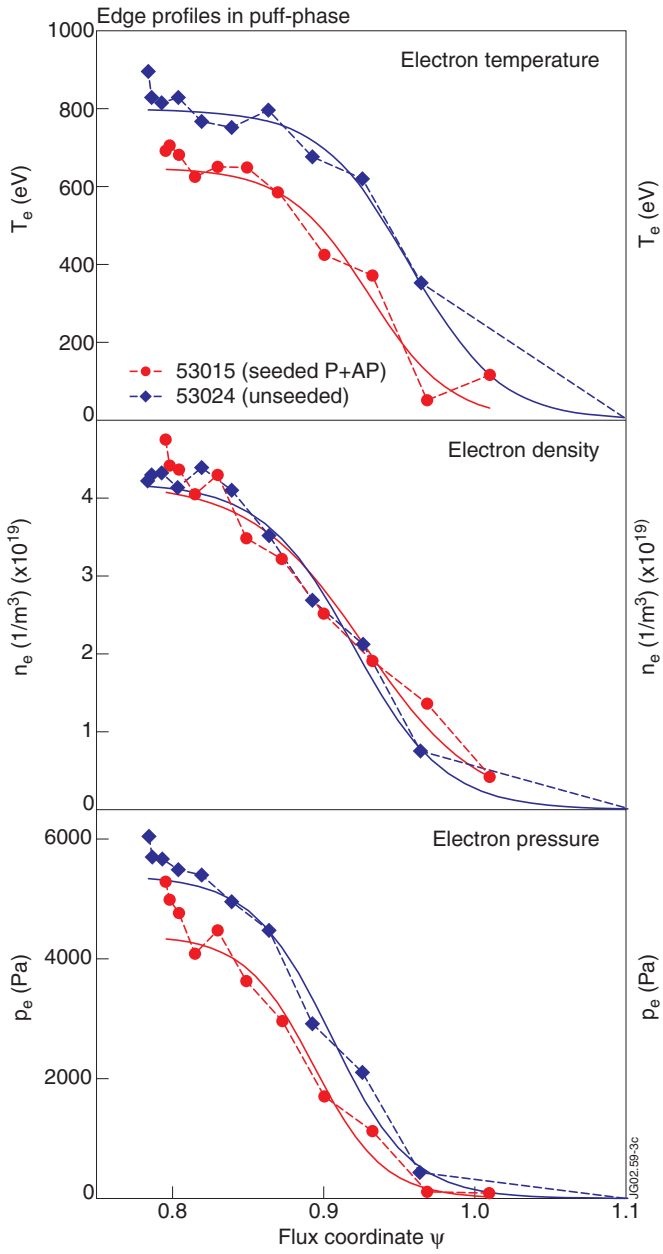

Figure 3: Edge profiles of seeded and unseeded pulse. The profiles are taken during the puff at the time as indicated in figure 2. The solid lines correspond to a tanh-fit, from which the parameters in Table 1 have been taken.

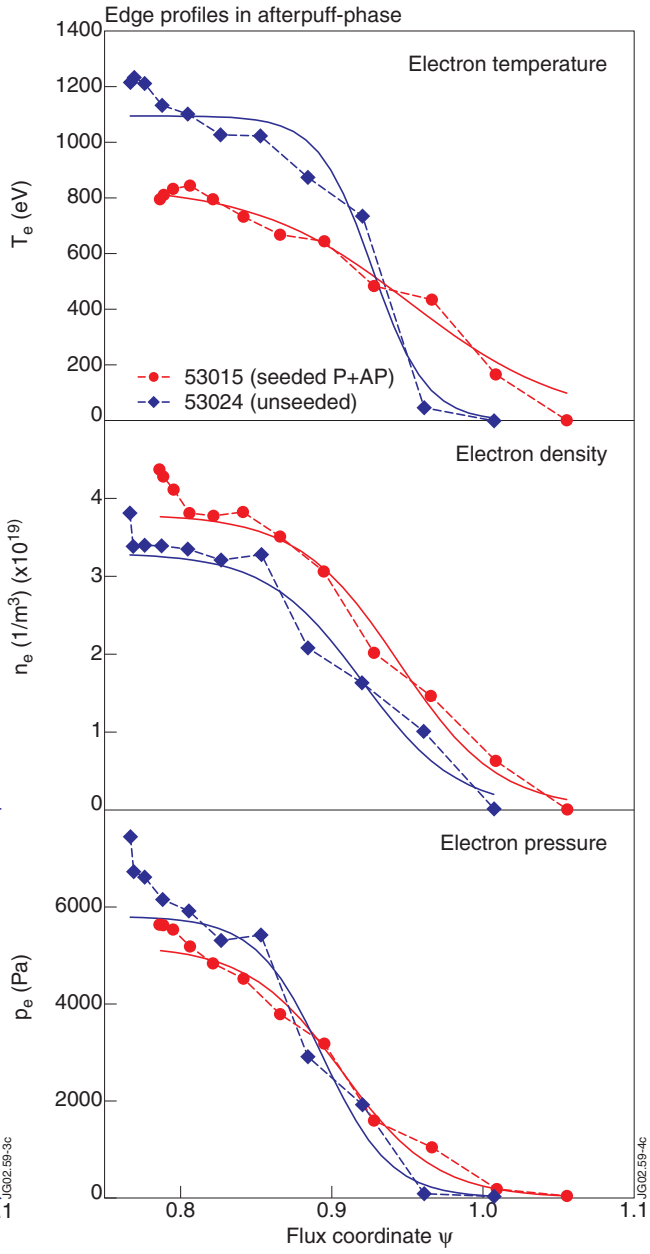

Figure 4: Edge profiles of seeded and unseeded pulse. The profiles are taken during the afterpuff phase at the time as indicated in figure 2. The solid lines correspond to a tanh-fit, from which the parameters in Table 1 have been taken.

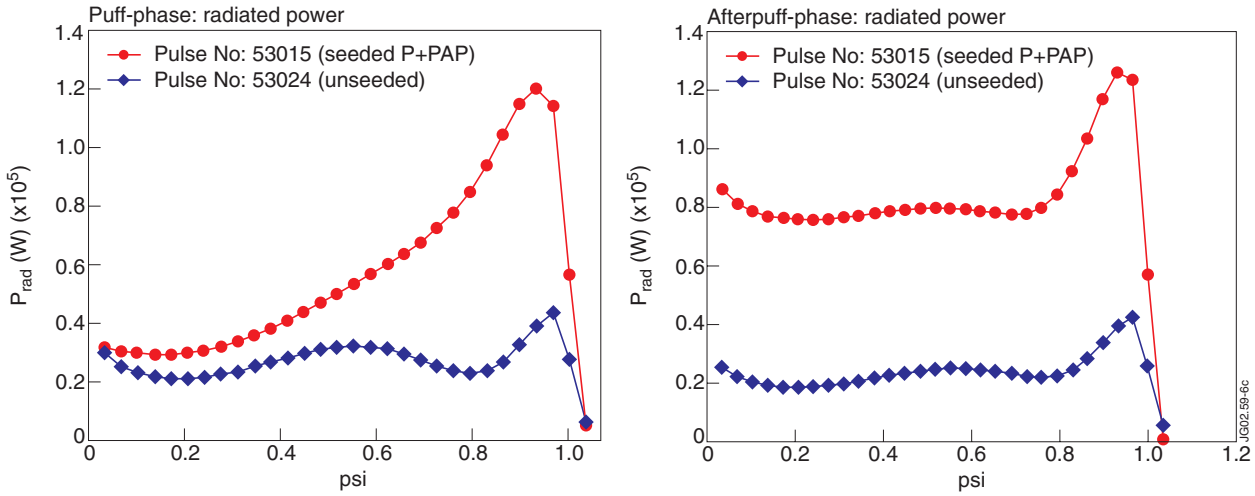

Figure 5: Abel inverted radiation profile during a) puff-phase and b) afterpuff-phase. Because of the seeding the radiation level increases from 20% to 50%.

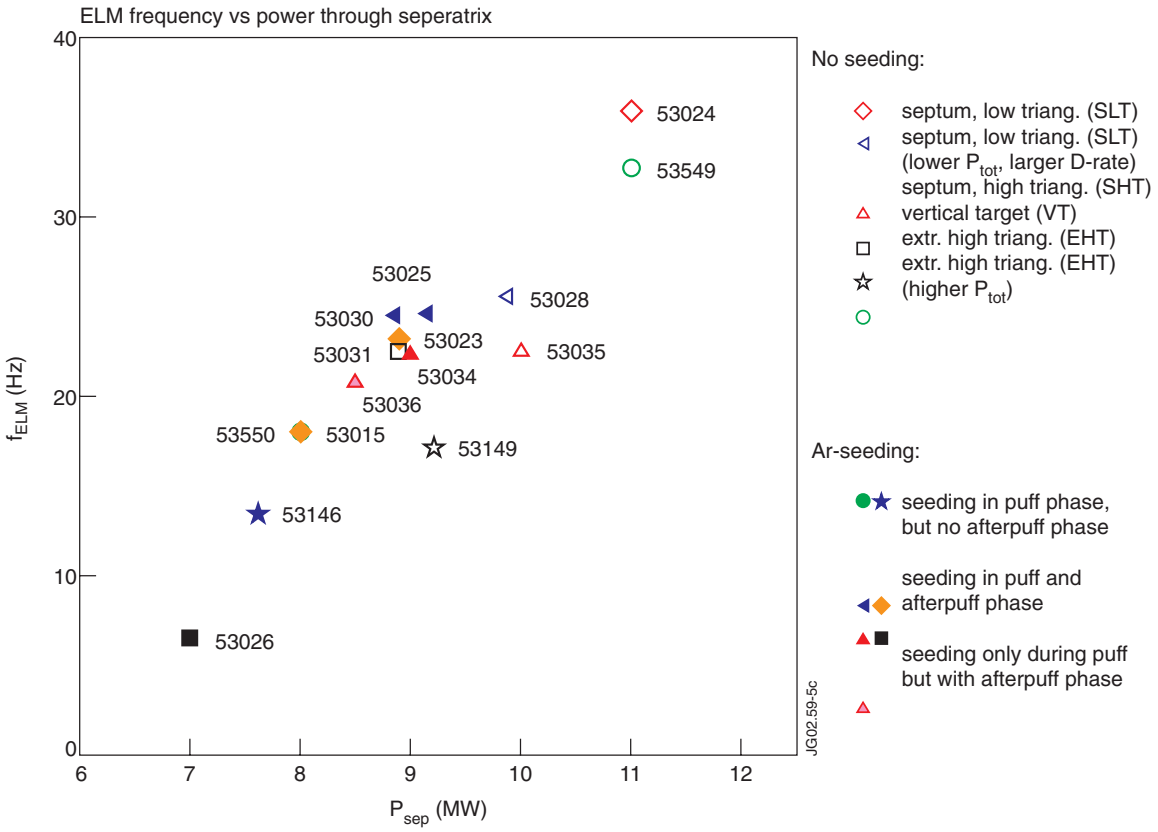

Figure 6: ELM frequency decreases with reduced power crossing the separatrix. The open symbols correspond to unseeded pulses, the closed to seeded one. Except for the EHT pulses all data correspond to the afterpuff-phase. In all cases shown here were Type I ELMs present.

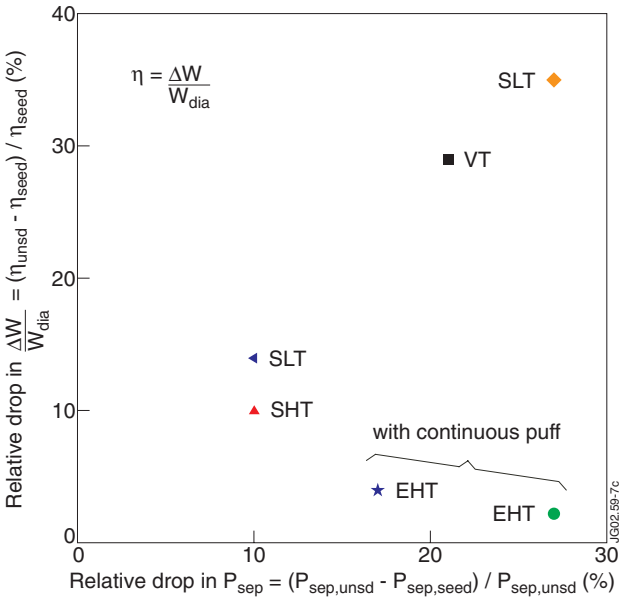

Figure 7: Relative drop in ELM energy loss fraction and separatrix power of seeded with respect to the unseeded pulse determined from the fast diamagnetic signal. The relative drop expresses by which amount the energy loss fraction changes for a certain decrease of the power crossing the separatrix.

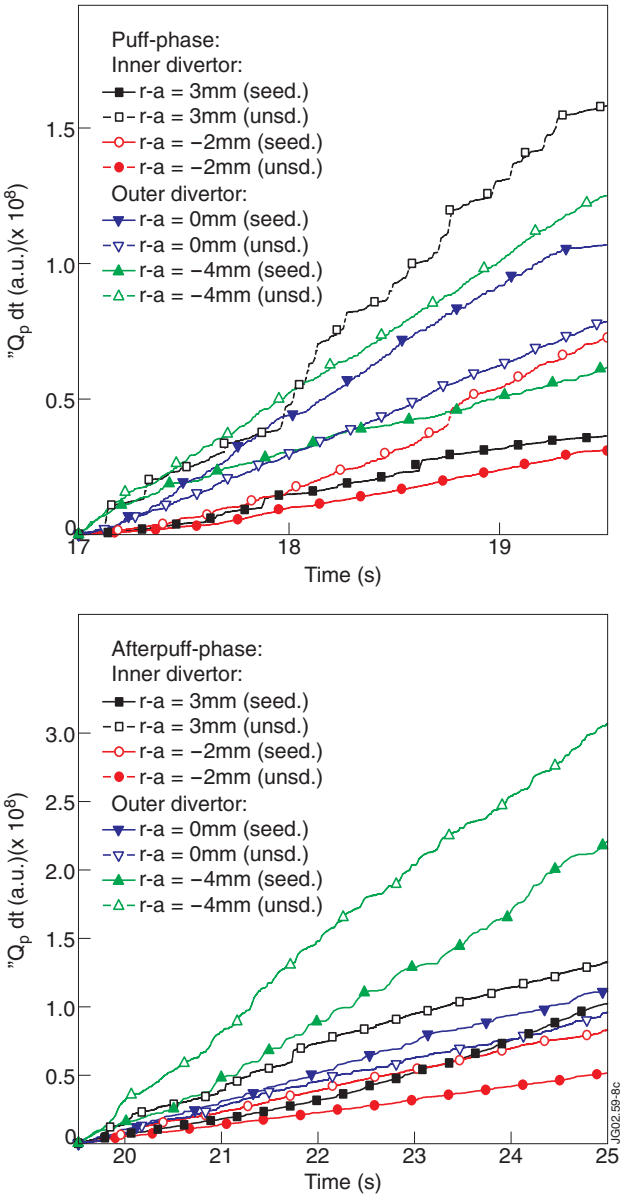

Figure 8: Accumulated heat flux as measured by the divertor Langmuir probes (VT: seeded=52161, unseeded=53031). Shown is the respective difference for (a) the puff-phase and (b) the afterpuff-phase. The closed symbols correspond to the seeded discharge, the open to the unseeded reference discharge. The quantity r-a is the position relatively to the strike point mapped to the midplane radius.

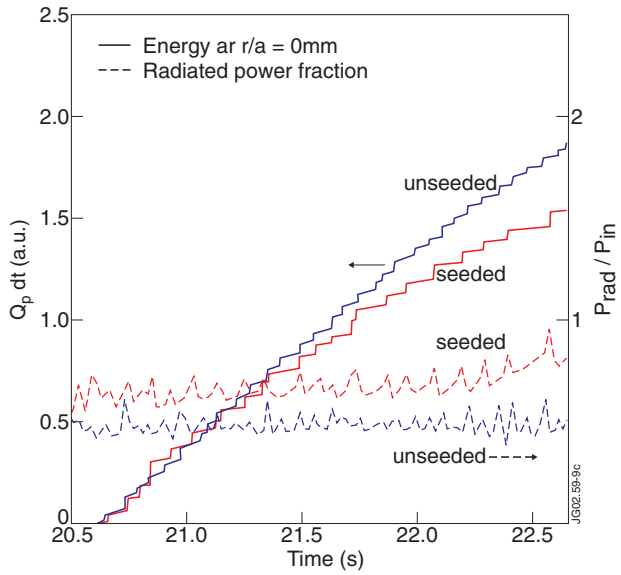

Figure 9: Time-integrated heat flux to the outer divertor as measured by a probe and the corresponding radiation levels. The pulses (seed.=53146, unsd.=53149) were in EHT configuration with a continuous D_2-puff.

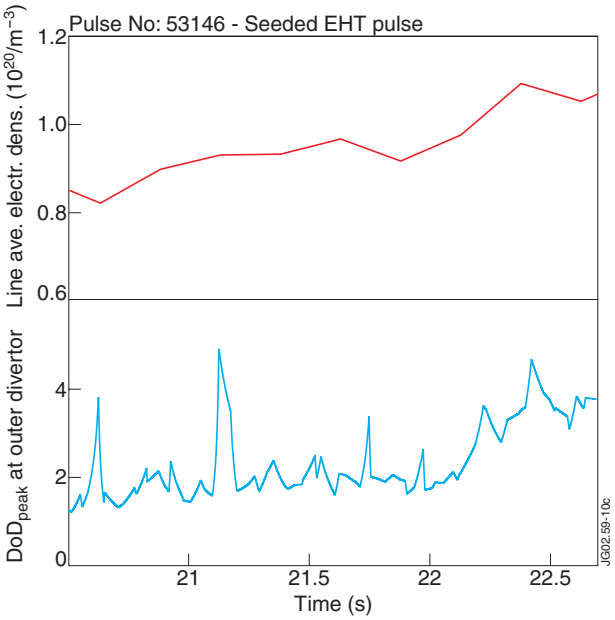

Figure 10: Time traces of (a) line averaged density during an EHT discharge and (b) Degree of detachment determined from a probe, which is located at the strike point. With the first increase of the radiation level at t=20.5 the DoD indicates that the outer divertor close to be at the attachment limit. Once the radiation level increases more at t=22.0 the outer divertor detaches.

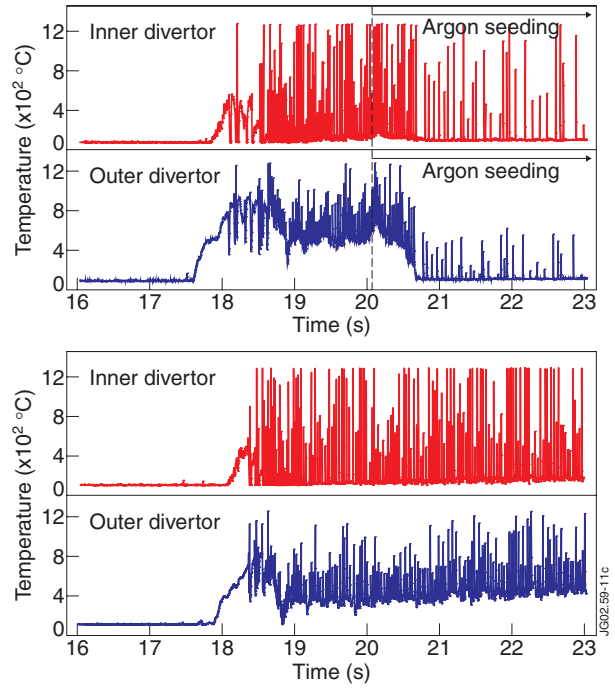

Figure 11: Surface temperature of the inner and outer divertor tiles in a seeded and unseeded EHT discharge. Soon after the seeding started the baseline temperature is reduced.

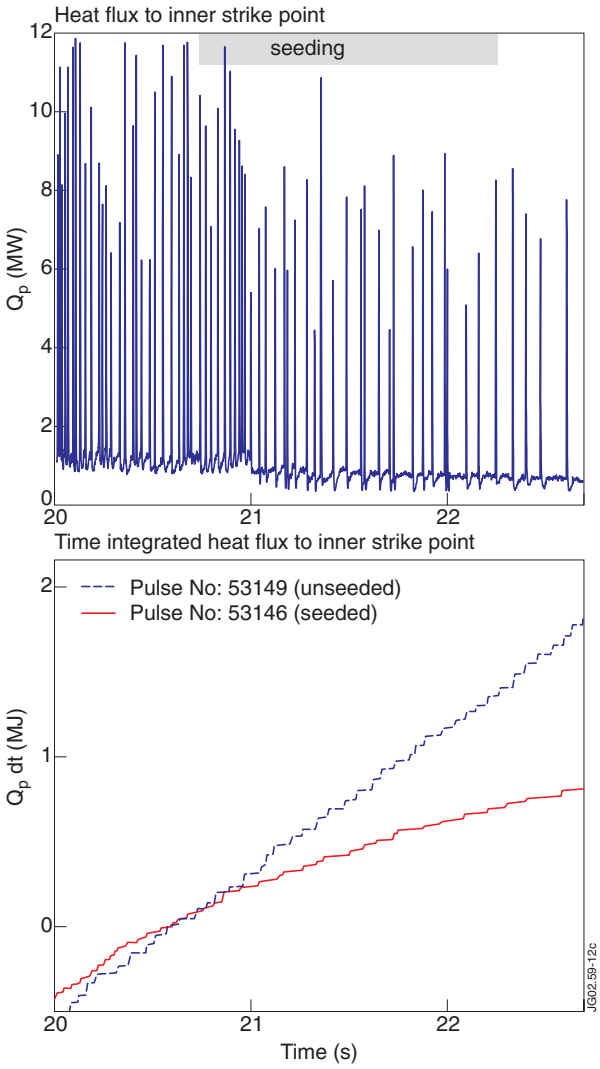

Figure 12: (a) Heat flux to the inner strike point of the seeded pulse and (b) the resulting time integrated heat flux in comparison with that of an unseeded pulse in EHT configuration. Once the seeding started, not only the in between ELM heat flux decreases but also the ELM-peaks are reduced by about 10%.